Neutron Irradiation Performance of Fe–Cr Base Alloys

James Stubbins – University of Illinois at Urbana-Champaign – jstubbin@illinois.edu

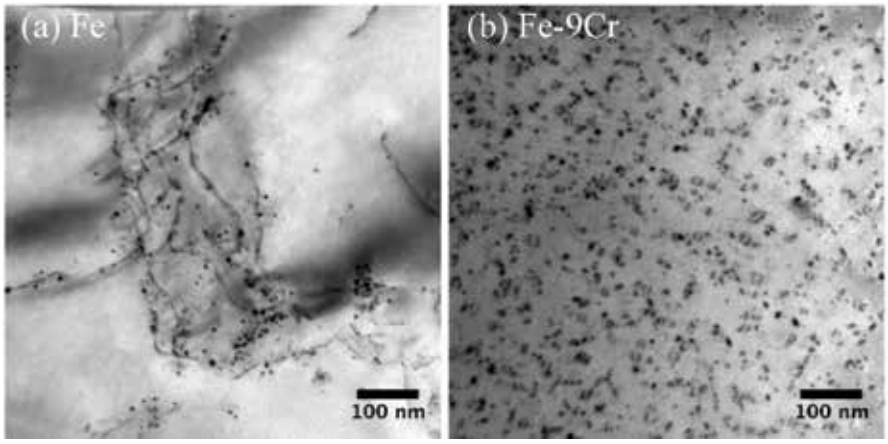

Figure 1. A comparison of (a) dislocation decoration in Fe irradiated to 1 dpa at 300°C, and (b) uniform dislocation loops in Fe–10Cr irradiated to 1 dpa at 300°C.

This project included several firsts including the first irradiations of low dose (0.01 and 0.1 dpa) specimens at ATR, first use of MR-CAT for in situ tensile tests of ATR specimens, and first use of NSUF facilities for Positron Annihilation Research.

Advanced nuclear reactors come with inherent safety and improved energy efficiency, but they also require harsh operating conditions, such as elevated temperatures, high-dose neutron exposure, and corrosive environment. Fe–Cr-base ferritic/martensitic (F/M) alloys are considered lead candidate materials for in-core (cladding, ducts, and wrappers) and out-of-core (pressure vessel, piping) structural applications in advanced reactors. Compared to austenitic alloys, F/M alloys have higher thermal conductivity, a lower thermal expansion coefficient, and superior resistance to swelling and helium embrittlement. However, at relatively low temperatures, F/M alloys are susceptible to irradiation hardening and embrittlement.

The irradiation hardening and embrittlement in F/M alloys are known to be related to two types of defects created by neutron irradiation: (1) dislocation loops and (2) precipitates such as Cr-rich α' phase, Ni, Mn, Si-rich G-phase, and Cu-rich phase. It is critical to understand the microstructural evolution and governing mechanisms, in order to design advanced radiation-resistant alloys that can meet the requirements of next-generation reactors.

Project Description

In this research program, a coordinated set of ATR neutron-irradiation experiments with post-irradiation examination (PIE) on Fe–Cr base alloys were carried out, and several rapid-turnaround experiment (RTE) projects focusing on the PIE of irradiated specimens are ongoing. The suite of alloys ranges from pure

Table 1. Target irradiation alloy matrix, specimen types, and exposure conditions.

Alloy	Temp (C)	Dose (dpa)	Specimen Types
Model Alloys Fe, Fe-9Cr, Fe-12Cr, Fe-14Cr, Fe-19Cr, also Fe-9Cr & Fe-12Cr with 0.1, 0.2 or 0.5 wt% C	300, 450, 550	0.01, 0.1, 0.5, 1, 5, 10	TEM, Miniature Tensile
Commercial Alloys T91, HT-9	300, 450, 550	0.01, 0.1, 0.5, 1, 5, 10	TEM, Miniature Tensile
Developmental Alloys MA-957	300, 450, 550	0.01, 0.1, 0.5, 1, 5, 10	TEM, Miniature Tensile

iron to Fe–Cr binary model alloys to Fe–Cr–C ternary model alloys to commercial and developmental alloys. This spectrum of simple-to-complex Fe–Cr base alloys provide the basis for assessing the underlying radiation performance processes even in complex alloy systems. The new level of understanding on the irradiation performance of this alloy system will also facilitate the development of modeling capabilities to better predict future alloy performance and development.

A set of state-of-the-art techniques has been used for the characterization of the irradiated alloys. Transmission electron microscopy (TEM), atom probe tomography (APT), and positron annihilation spectroscopy (PAS) were used to characterize the irradiated microstructure. Nanoindentation and *in situ* synchrotron wide-angle X-ray scattering (WAXS) were used to study mechanical properties. Figure 1 is an example of TEM results comparing the loop structure of iron (Fe) and Fe–9Cr alloy that underwent the same neutron irradiation. It is clear that in Fe the dislocations are decorated by small black-dot dislocation loops, and in Fe–9Cr a homogeneous loop structure was observed. The reason is that the addition of chromium reduces the mobility of a/2 ⟨111⟩ loops and prevents them from migrating to pre-existing dislocations, resulting in a uniform loop distribution.

Another important feature commonly observed in irradiated high-Cr ferritic alloys are Cr-rich α' precipitates. Previous studies indicated that α' precipitation is a radiation-enhanced process, rather than radiation-induced. Interestingly, the α' precipitation was found highly dependent on the bombarding radiation particles and

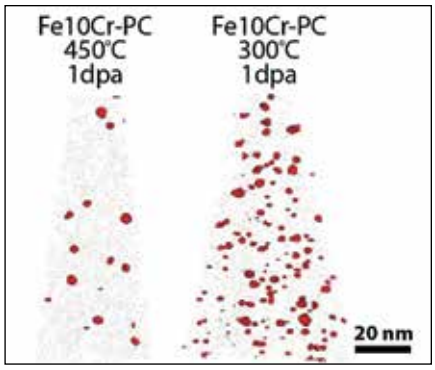

Figure 2. 20 at.% Cr isosurfaces showing the α' precipitates in neutron-irradiated Fe-10Cr samples.

dose rate: α' precipitation was hardly observed in high-dose-rate heavy-ion-irradiated Fe–Cr alloys, but was observed in proton-, electron-, or neutron-irradiated Fe–Cr alloys. The chromium content of Cr-rich precipitates found in several studies is way below phase-diagram prediction, indicating strong effects due to ballistic mixing. Figure 2 shows the α' precipitates found in neutron-irradiated Fe–9Cr at two different irradiation temperatures. The decreasing number density of α' precipitates with increasing irradiation temperature agrees with the phase diagram. However, the chromium content of these α' precipitates is also found to be considerably lower than the values predicted by the phase diagram.

Microstructure characterization of HT9 and T91

HT9 (12Cr) and T91 (9Cr) are high Cr F/M steels of great interest for applications in advanced reactors. In this project the specimens were irradiated to a relatively low dose level and then characterized using TEM and APT. The mechanical properties were measured by nanoindentation. A variety of radiation-induced microstructural changes were observed, including dislocation loops, radiation-induced precipitation, and segregation. The irradiation doses and thermal conditions were estimated using simulation methods, and the conditions investigated in this project are shown in Figure 3.

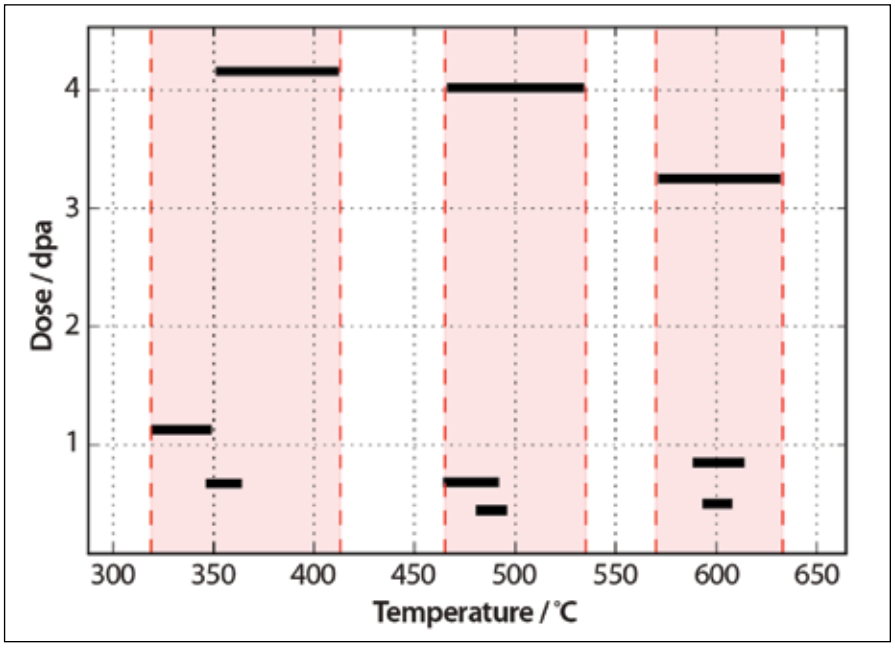

Figure. 3 Temperature and dose range of the irradiated HT9 and T91 specimens investigated.

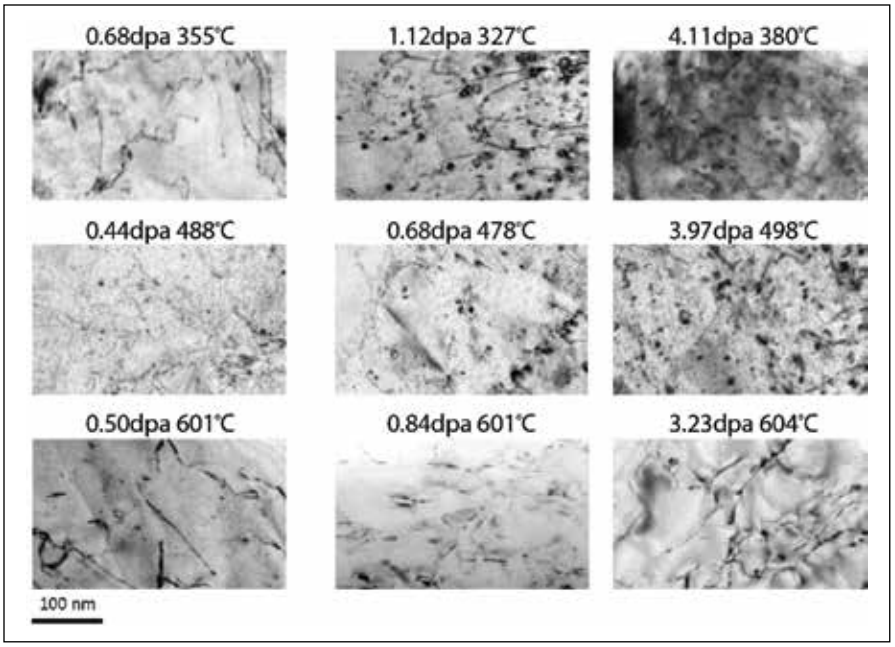

Figure 4. Effect of dose and temperature on the structure in T91.

Radiation-induced defect microstructures

Both TEM and STEM were used to characterize irradiation-induced dislocation-loop structures in T91. Most TEM samples were prepared using an electropolishing technique. For the conditions where electropolished specimens were not available, the FIB lift-out technique was used to prepare the samples for TEM experiments.

The damage microstructures in T91 under various irradiation conditions are shown in Figure 4. The defect evolution in HT9 is similar to T91. The sizes of the dislocation loops strongly depend on the irradiation temperature, where the largest dislocation loops were observed at the highest temperature. Under the similar dose level, at low temperature (around 350°C), damage was only visible above 1 dpa (except under special weak beam imaging conditions). At higher temperatures, visible loops were observed as early as 0.44 dpa. Considering the actual highest irradiation temperature is above 600°C, minimum irradiation damage was expected due to multiple factors including high-point defect recombination rate, low defect-cluster nucleation rate and thermal recovery above 600°C. On the contrary, significant irradiation damage was observed in this temperature regime. We also observed small loops with an average

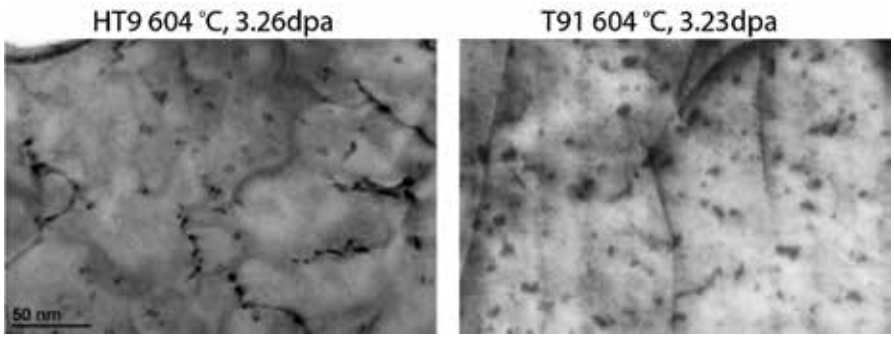

Figure 5. Small loops observed in HT9 and T91 following high temperature high dose irradiation.

size of around 5 nm in the samples irradiated at highest temperature of 604°C and 3 dpa (see Figure 5).

The abnormal defect structure is further illustrated by the multimodal size distribution of dislocation loops in samples irradiated for more than one cycle in the medium temperature range of 400 to 500°C. These phenomena can be explained by the lack of temperature control in reactor irradiation experiments. The specimens were sealed in capsules, and the main heating mechanism was by prompt gamma heating. The irradiation temperature was not well controlled during the experiment.

The samples may have experienced a fair amount of low-temperature irradiation, which leads to significant defect-cluster nucleation. These small clusters will then rapidly grow and develop into the scenario observed. The size of the dislocation loops is summarized in Figure 6 as a function of dose at 350°C. At low-temperatures, the loop sizes are similar in two materials, while the loops are significantly larger in T91 at higher temperatures, suggesting faster loop growth.

Radiation-induced segregation (RIS)

STEM-EDS and APT were used to analyze radiation-induced segregation (RIS) and precipitation. Significant segregation of Cr, Si, Ni, Mn, P, and

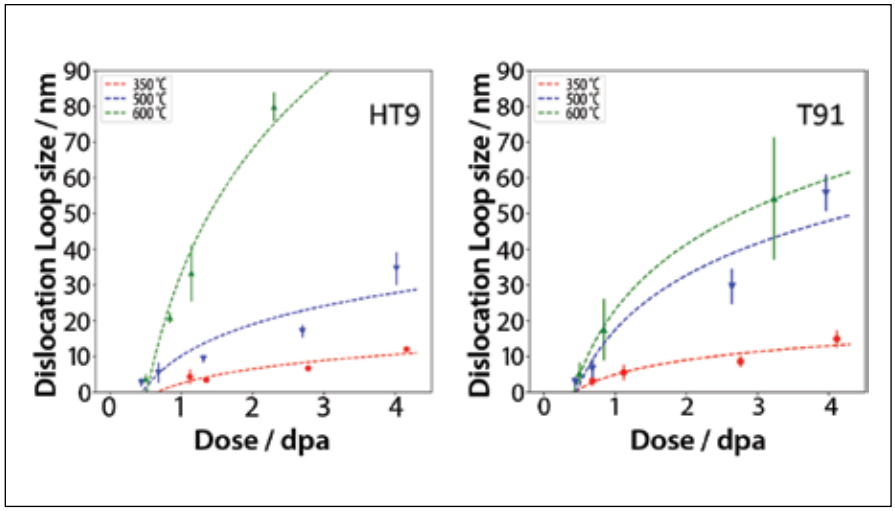

Figure 6. Dislocation loop size in HT9 and T91 irradiation at 350, 500 and 600°C.

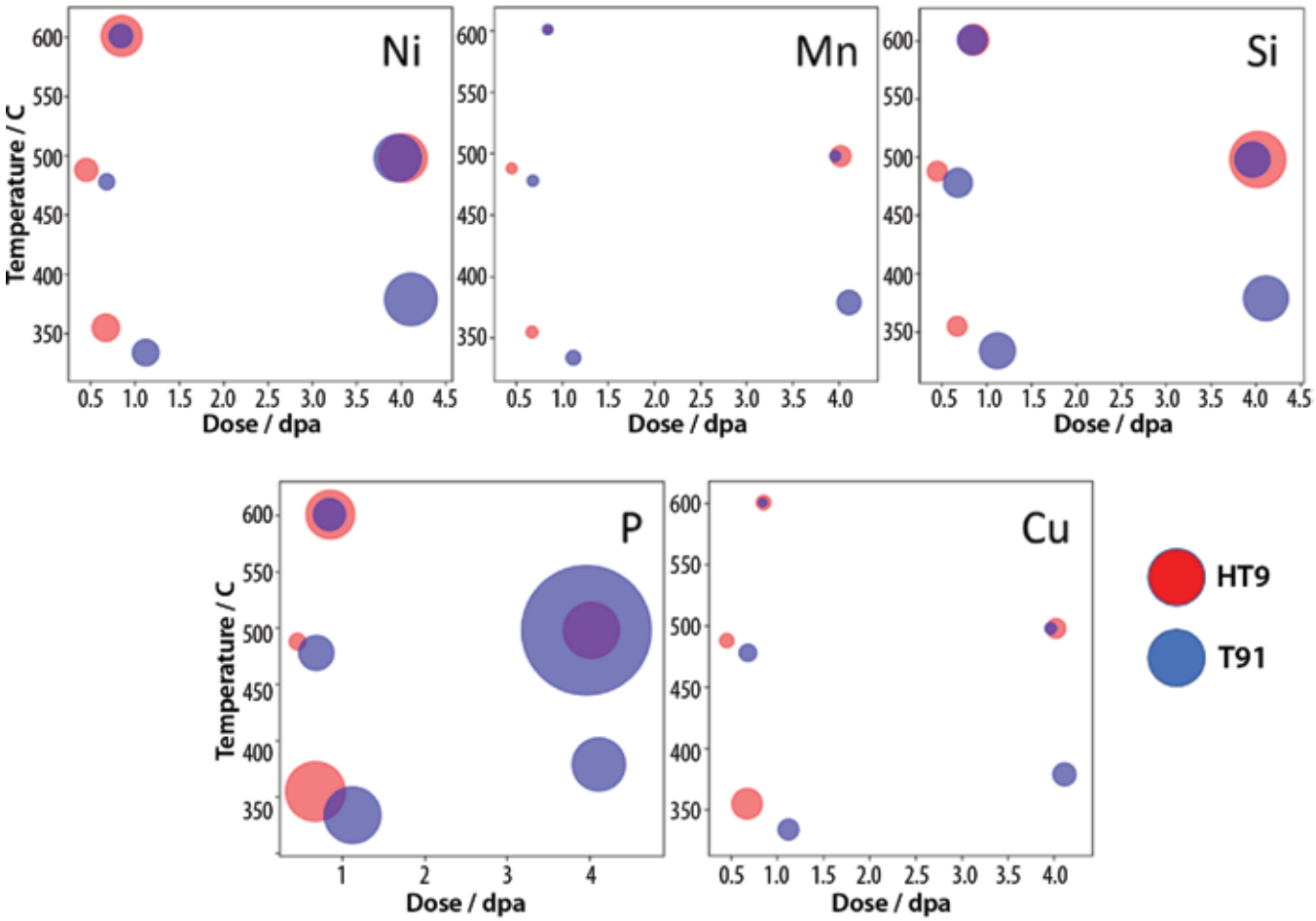

Cu was observed in some conditions at grain boundaries (Figure 7), second-phase boundaries, and dislocations. The dose dependency can be observed for Ni, Mn, Si, P, and Cu, but the temperature dependency is not clear. Strong segregation at the highest temperature might originate from the lack of temperature control. The highest RIS is observed for the element P, with the peak concentration 44 times higher than the bulk concentration. The segregation of Ni, Mn and Si contributes to the precipitation of G-phase. The segregation of Cr to nitride surfaces facilitates the transformation of nitrides.

Figure 7. RIS of minor elements on GBs in HT9 and T91 as a function of dose and irradiation temperature. The radius of the circles is proportional to the percentage concentration increase.

Radiation-induced Precipitation

A variety of radiation-induced modifications of the precipitation processes was observed, including the precipitation of G-phase, α', Cu-rich phase and modification of nitrides.

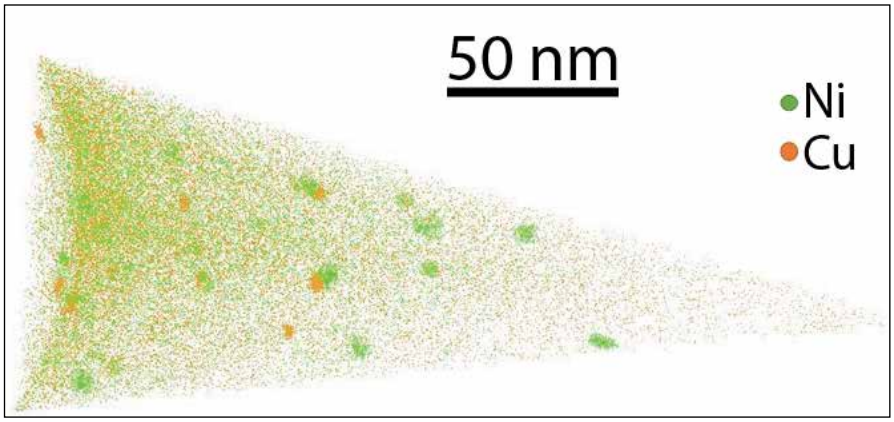

Figure 8. Ni atom maps showing the size and distribution of G-phase in irradiated HT9.

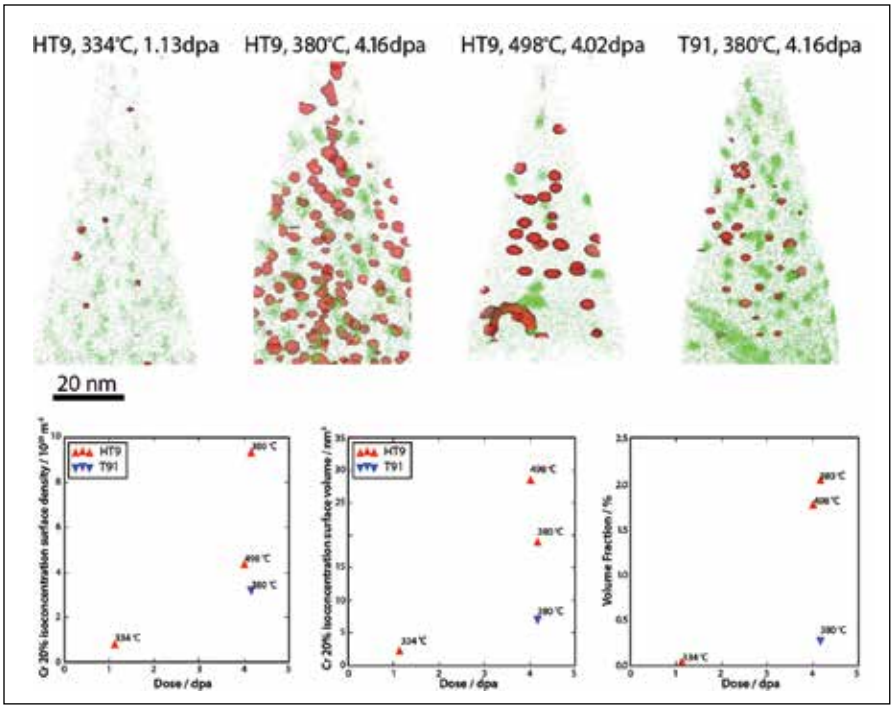

Figure 9. The distribution of α' visualized by 20% Cr isoconcentration surfaces. The size, density and volume fraction are also shown.

G-phase is a Ni-rich silicide frequently observed in irradiated steels due to the radiation-induced segregation of Ni, Mn and Si. The spatial distribution of G-phase particles is visualized in Figure 8 using APT Ni mapping. We analyzed the particles using Ni, Si, Mn isoconcentration surfaces. The concentration evolution with irradiation is illustrated in Figure 9. The Ni, Si ratio is close to 1 for low-dose specimens, suggesting similar RIS for these two elements. The ratios then converge to the G-phase ratio, confirming that the particles are G-phase.

Cr-rich α' precipitates were also observed in HT9 and T91 under certain conditions. The precipitation of α' agrees well with the previously published results. In the 12Cr steel HT9, α' was observed in both low and medium temperature ranges, while in 9Cr steel T91, it was only observed in the low temperature range. The APT images and the size, density and volume fraction of α' are shown in Figure 9.

A Cu-rich phase was observed in T91 (Figure 11). Even though RIS of Cu was also observed in HT9, no clearly defined clusters of Cu were found in HT9. In T91 irradiated at high temperature to 3.23 dpa, Cu-rich particles were the only small-scale precipitates observed in APT. In the medium temperature range, G-phase and Cu-rich phase coexist and appear to have spatial correlations (See Figure 10). Nitrides are important precipitates in this type of steel. The most prominent type of nitrides in HT9 and T91 is vanadium nitride (VN). The thermodynamic calculation shows that VN is not a stable phase. Instead CrVN (Z phase) is the stable phase in high Cr steels. We observed the RIS of Cr on the VN phase boundary (Figure 12) and the modification of such phase. Cr_2N was also observed at both materials in low temperatures after

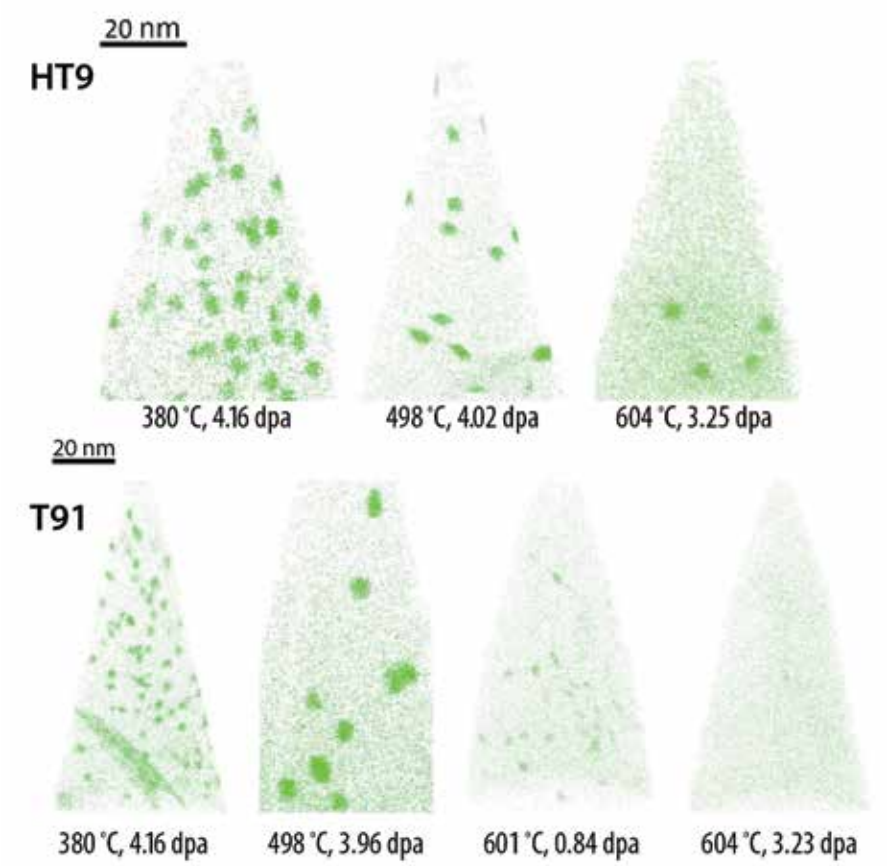

Figure 10. G-phase and Cu-rich phase coexist in irradiated HT9 and T91 over the medium temperature range.

long-term irradiation, up to 10 dpa. In general, three types of nitrides were identified in HT9 and T91, including VN, Z phase, and Cr_2N.

In addition to the model and F/M alloys, PIE work on an irradiated Fe–14Cr-base ferritic oxide dispersion strengthened (ODS) alloy MA957 has also started. Currently, microstructure characterization has been completed. Few dislocation loops were found in the lowest-dose specimens, and large loops were only found in the highest-dose specimens. The loops found in the intermediate dose (1.02 dpa at 340°C and 0.69 dpa at 478°C) were small black-dots. It might be possible to divide the loop evolution into two regimes: loop nucleation below ~1 dpa, and loop growth above ~1 dpa.

Since MA957 is a Fe–14Cr alloy, the Cr content is above the threshold value for α' precipitation, which can be accelerated by neutron irradiation. Indeed, α' precipitation was observed in irradiated MA957 at several irradiation conditions. The α' precipitates can be readily seen from the Cr atom maps at the highest dose. More detailed analysis using Cr isosurfaces show that some α' precipitates can also be found in the ~1 dpa specimens.

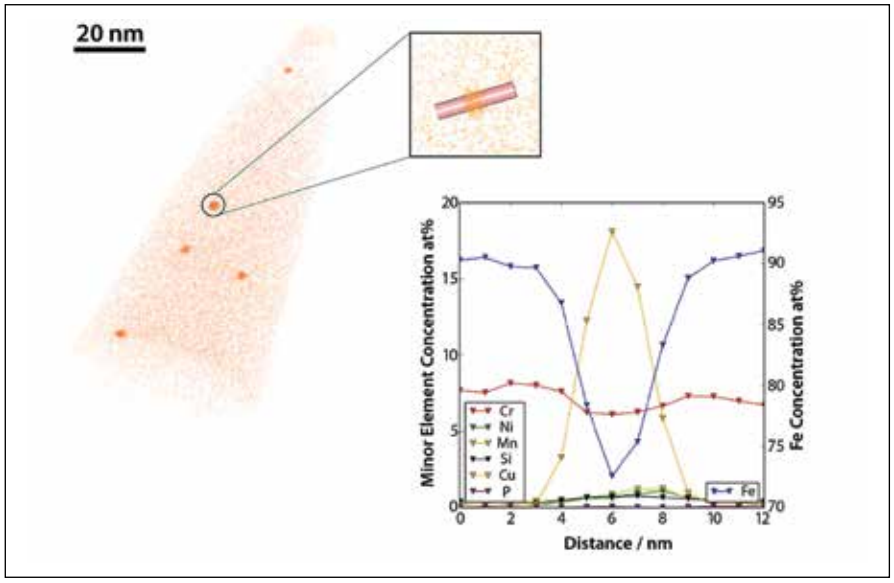

Figure 11. Cu-rich precipitates found in T91 irradiated around 600°C to 3.23 dpa

In Situ tensile tests with synchrotron X-ray diffraction

To study the irradiation embrittlement on F/M alloys, *in situ* synchrotron X-ray diffraction (XRD) measurements of the tensile deformation of irradiated samples were conducted. Because the samples were irradiated by neutron and activated with various radioactive isotopes, special confinement techniques were required to prevent radioactive contamination of the Advanced Photon Source (APS) beamline areas. Two types of radiation-confinement methods were developed for the *in situ* APS experiment. In APS beamline 1-ID, we employed double-contained encapsulation for irradiated samples on the universal tensile machine. For the APS beamline 10-ID experiment, glovebox type confinement system was designed to enclose the samples and all experimental stages.

An *in situ* tensile test with high-energy X-ray provides more profound information over a conventional tensile test, including elastic and plastic behaviors with connections to specific crystal planes.

The lattice strains generated under applied stresses were mainly due to the elastic properties with *hkl* planes and plastic deformation with crystal slip planes and slip directions. Dislocation loops and the α' precipitation are the major contributors of irradiation hardenings. The theoretical contributions to

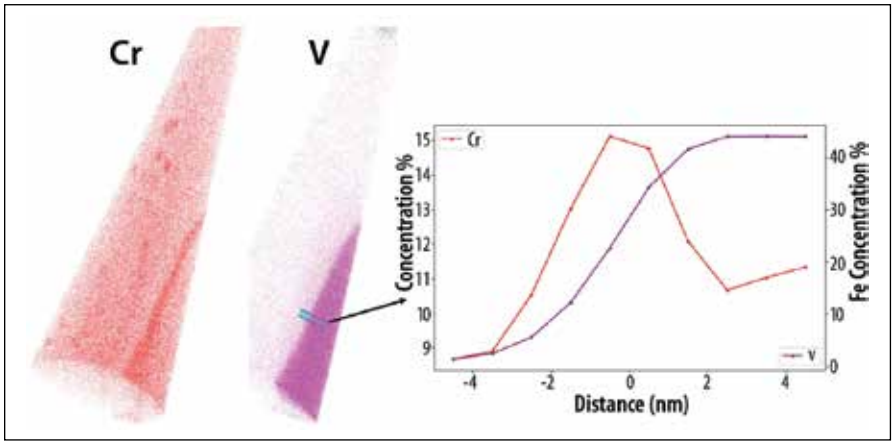

Figure 12. Cr RIS at VN phase boundary.

irradiation hardening by dislocation loops and the α' precipitation can be calculated by dispersed barrier hardening models.

The hardening contribution of the α' precipitation is a relatively simple function of density and average diameter of α' precipitations observed in APT. The calculation of irradiation hardening by dislocation loops, on the other hand, requires more-advanced modeling that consider the influence of critical resolved-shear stress on slip systems, habit planes of dislocation loops, and dislocation-density evolution during deformation.

Another major advantage of performing *in situ* synchrotron XRD tensile testing is that dislocation-density evolution during deformation can be obtained using the Williamson-Hall analysis. The *in situ* tensile study shows similar plasticity behaviors in the low-dose samples and substantially increases dislocation densities at the higher dose samples.

HEDM (High-energy X-ray diffraction microscopy)

High-energy diffraction microscopy (HEDM) is a non-destructive three dimensional XRD technique that is suitable to characterize mechanical properties of neutron-irradiated samples. The APS 1-ID beamline has developed HEDM to obtain *in situ* grain-by-grain tensile behavior. Near-field high-energy diffraction microscopy (nf-HEDM) is used to obtain a crystallographic-orientation map of grains. Far-field high-energy diffraction microscopy (ff-HEDM) uses the high-resolution detector in ways similar to the WAXS detector to

This spectrum of simple-to-complex Fe–Cr base alloys will provide the basis for assessing the processes underlying radiation performance even in complex alloy systems.

obtain grain-resolved lattice strains. The combination of nf-HEDM and ff-HEDM allows analyzing the distributions of orientations and strains at the scale of the sub-grain.

Because HEDM provides a crystallographic orientation map at microscale resolution, it is possible to obtain distributions of local misorientation in a grain. Local misorientations indicate local strains, usually plastic strains, because dislocations accompany residual strain and alter lattice orientations. Kernel average misorientation (KAM) is the popular approach to calculate variations of intergranular lattice orientations in electron backscatter diffraction, and it can be adapted to HEDM. KAM is numerically defined as the average misorentations between all neighboring kernels within the kernel. In the case that some kernels include grain boundaries, the kernels with KAM ≥5 degrees, for example, are excluded from the averaging calculation.

Positron annihilation studies

Positron Annihilation Spectroscopy (PAS) provides a mechanism for probing very small defect structures produced during irradiation. This technique is important since it is able to measure defects with dimensions smaller than those that can be imaged using even the highest resolution TEM techniques. PAS has the ability to identify the presence of these tiny clusters, particularly vacancy clusters. This is critical to help develop a basis for understanding the void nucleation and void incubation processes, about which very little is presently known. Thus, PAS can provide an important link to the modeling of damage evolution. In addition to the role in damage structure evolution, the invisible defects, when they exist, can have an important impact on dislocation movement and overall deformation behavior.

This research is ongoing with the lowest-dose samples from the ATR irradiations.

Accomplishments

At present, a series of experimental and modeling work has been accomplished. Neutron irradiation on both disc specimens and miniature tensile specimens has been completed. The target doses range from 0.01 to 10 dpa (completed in six cycles), and the target temperatures were 300, 450, and 550°C. For PIE on neutron-irradiated specimens, advanced characterization and testing techniques have been employed to explore the relationship between irradiated microstructure and mechanical properties.

Several RTE projects and a two-year Nuclear Science User Facilities (NSUF)-access-only project on microstructure characterization (TEM and APT) have been completed on neutron-irradiated Fe, Fe–Cr binary model alloy, Fe–9Cr–0.1C and Fe–9Cr–0.5C ternary model alloys, complex F/M alloys T91, HT9 and ODS MA957. The PIE work spans over 6 years, and TEM characterization was carried out using several electron microscopes at multiple facilities: MaCS (FEI Tecnai TF30-FEG STwin STEM) at the Center for Advanced Energy Studies (CAES), the Electron Microscopy Laboratory at Idaho National Laboratory (INL) (JEOL 2010 LaB6 TEM), Irradiated Materials Characterization Laboratory at INL (FEI Titan Themis 200 FEG-STEM), and the Low Activation Materials Design and Analysis Laboratory at Oak Ridge National Laboratory. The APT characterization was carried out using a LEAP 4000× HR at MaCS.

Collaborating with two beamlines (1-ID and MRCAT 10-ID) at Argonne National Laboratory's APS, *in situ* tensile tests with synchrotron WAXS and small-angle X-ray scattering (SAXS) have been completed on both control samples and neutron-irradiated Fe, Fe–9Cr, Fe–9Cr–0.1C, Fe–9Cr–0.5C, Fe–12Cr–0.2C, and Fe–12Cr–0.5C alloys. For the experiments at the Materials Research Collaborative Access Team, a customized glovebox was built for the *in situ* tensile tests. This set of novel experiments will provide significant new insights on the effects of neutron irradiation on the microstructure and plastic deformation mechanisms.

An RTE project on measuring the nanohardness of neutron-irradiated Fe–Cr–C model alloys has also been completed, through collaboration with Dr. Peter Hosemann's Nuclear Materials Laboratory at University of California, Berkeley. The data are being used to correlate the irradiated microstructure with changes in mechanical property.

An NSUF-access-only project has also been initiated with North Carolina State University to measure the early stage of defect evolution in low-dose (e.g., 0.01 dpa and 0.1 dpa) specimens using PAS. At such low doses, a significant fraction of defects produced by neutron irradiation has not evolved into clustered form that can be resolved by conventional TEM. The PAS technique offers the possibility to examine small vacancy-type clusters. The experiments are ongoing at North Carolina State University.

Future Activities

Further investigations on the remaining neutron-irradiated specimens that will help bridge the knowledge gap from simple model alloys to complex F/M alloys will be carried out through future funding from NSUF RTE projects, NSUF-access-only projects, and Nuclear Energy University Program/Nuclear Energy Enabling Technology projects. Although efforts have been made to get microstructure data (including TEM, APT, PAS), nanoindentation, synchrotron WAXS/SAXS tensile data on the same set of irradiated samples, there is still a long way to go to perform such coordinated experiments using the state-of-the-art facilities at different national labs. We will push forward with the PIE efforts to make such experiments happen to advance the understanding of radiation effects in ferritic and F/M alloys.

Publications

[1.] X. Liu, Y. Miao, Y. Wu, S.A. Maloy, J.F. Stubbins, "Stability of nanoclusters in an oxide dispersion strengthened alloy under neutron irradiation", Scripta Materialia 138 (2018) 57–61.

[2.] X. Zhang, M. Li, J.-S. Park, P. Kenesei, J. Almer, C. Xu, J.F. Stubbins, "*In situ* high-energy X-ray diffraction study of tensile deformation of neutron-irradiated polycrystalline Fe-9%Cr alloy", Acta Materialia 126 (2017) 67–76.

[3.] W.-Y. Chen, Y. Miao, J. Gan, M.A. Okuniewski, S.A. Maloy, J.F. Stubbins, "Neutron irradiation effects in Fe and Fe–Cr at 300°C", Acta Materialia 111 (2016) 407–416.

[4.] X. Liu, K. Mo, Y. Miao, K.-C. Lan, G. Zhang, W.-Y. Chen, C.A. Tomchik, R. Seibert, J. Terry, J.F. Stubbins, "Investigation of thermal aging effects on the tensile properties of Alloy 617 by in-situ synchrotron wide-angle X-ray scattering", Materials Science and Engineering: A 651 (2016) 55–62.

[5.] W.-Y. Chen, Y. Miao, Y. Wu, C.A. Tomchik, K. Mo, J. Gan, M.A. Okuniewski, S.A. Maloy, J.F. Stubbins, "Atom probe study of irradiation-enhanced precipitation in neutron-irradiated Fe–Cr model alloys", Journal of Nuclear Materials 462 (2015) 242–249.

Distributed Partnership at a Glance	
NSUF and Partners	Facilities and Capabilities
Argonne National Laboratory	The Intermediate Voltage Electron Microscopy (IVEM) – Tandem Facility
Center for Advanced Energy Studies	Microscopy and Characterization Suite (MaCS)
Idaho National Laboratory	Advanced Test Reactor (ATR), Irradiation Materials Characterization Laboratory (IMCL)
Illinois Institute of Technology	Materials Research Collaborative Access Team (MRCAT) facility at Argonne National Laboratory's Advanced Photon Source
North Carolina State University	PULSTAR Reactor Facility
Oak Ridge National Laboratory	Low Activation Materials Design and Analysis Laboratory (LAMDA)
University of California, Berkeley	Nuclear Materials Laboratory
Collaborators	
Argonne National Laboratory	Carolyn Tomchik (collaborator), Jonathan Almer (collaborator), Jun-Sang Park (collaborator), Kun Mo (collaborator), Meimei Li (collaborator), Mike Billone (collaborator), Wei-Ying Chen (collaborator), Xuan Zhang (collaborator), Yinbin Miao (collaborator)
Idaho National Laboratory	Assel Aitkaliyeva (collaborator), Collin Knight (collaborator), Jian Gan (collaborator), Lingfeng He (collaborator), Xiang Liu (collaborator),
Illinois Institute of Technology	Jeff Terry (collaborator)
North Carolina State University	Ayman Hawari (collaborator), Ming Liu (collaborator), Scott Lassell (collaborator)
Los Alamos National Laboratory	Stu Maloy (collaborator)
University of California, Berkeley	Peter Hosemann (collaborator)
University of Illinois at Urbana-Champaign	James Stubbins (principal investigator)